Salvador, F.J.; Ruiz, S.; Salavert Fernández, JM.; De La Morena Borja, J. (2013). Consequences of using biodiesel on the injection and air-fuel mixing processes in diesel engines. Proceedings of the Institution of Mechanical Engineers, Part D: Journal of Automobile Engineering. 227(8):1130-1141. doi:10.1177/0954407012463667.

CONSEQUENCES OF USING BIODIESEL ON THE INJECTION AND AIR-FUEL MIXING PROCESSES IN DIESEL ENGINES

Salvador, F.J. (*); Ruiz, S.; Salavert, J.M.; De la Morena, J.

CMT- Motores Térmicos.

Universitat Politècnica de València.

Camino de Vera s/n, 46022, Valencia (Spain)

(*) Corresponding author:

Dr. F. J. Salvador, fsalvado@mot.upv.es

CMT-Motores Térmicos, Universidad Politécnica de Valencia

Camino de Vera s/n, E-46022, Valencia, Spain

Telephone: 34-963879659

Fax: 34- 963877659

ABSTRACT

A study of the injection process and spray behavior has been made for three different fuels. In particular, blends of rapeseed methyl ester (RME) with standard diesel fuel at 5% and 30% of biodiesel have been used for the current study, as well as pure RME. Hydraulic characterization of an 8-hole nozzle has been carried out using these three fuels, in order to explore and analyze the influence of fuel properties on mass flow rate and momentum flux at the nozzle exit. Additionally, spray visualization tests have been made in order to get information about spray cone angle, which allows the characterization of air-fuel mixing process. Finally, a theoretical derivation has been used to obtain further details of the microscopic characteristics of the spray and compare air-fuel mixing efficiency for the different biodiesel blends.

KEYWORDS: Diesel, biodiesel, spray, discharge coefficient, air-fuel mixing

1. INTRODUCTION

The use of biofuels is considered a possible solution for two of the most important challenges for the energy production and transportation industries: the reduction of the dependence on fossil fuels and the control of the environmental impact of engines.

Biodiesel is currently produced from vegetable oils and from others sources such as, algae, animal fats and residual oils which are gaining increasing importance and will constitute the main sources in the future.

In this sense, the effects of using biodiesel on pollutant emissions and engine performance have been widely studied over the last few years [1-6]. Lapuerta *et al*. [7] have recently made a review of these studies, leading to the following conclusions:

- At full load conditions, lower power is obtained when running an engine with biodiesel fuels, due to their lower heating value. At partial load operation, this effect is compensated with lower fuel consumption in the case of biodiesel, so that generated power becomes similar.
- Nitrogen oxides emissions are slightly higher for biodiesel fuels in general terms.
- Soot generation and emissions are considerably reduced due to the higher oxygen content and absence of aromatic components in biodiesel. Nevertheless, an undesirable effect is that the emitted particles also have smaller diameters.

There are still important knowledge gaps with respect to the influence of using biofuels on the physical phenomena involved with the injection process, such as internal nozzle characteristics or atomization process. These aspects have been extensively studied for regular diesel fuels due to their strong effect on air-fuel mixing efficiency and combustion development. In this sense, several authors have studied the influence of

nozzle geometry and fuel properties on internal nozzle flow characteristics [8-10]. Furthermore, flow characteristics at the nozzle exit have been shown to determine spray behavior, both under evaporative and non-evaporative conditions [10-13]. It is expected that the use of fuels with different properties would have significant effect in the air-fuel mixing process and combustion behavior.

In the current paper, an analysis of the mixing process efficiency was done for three different diesel fuel-rapeseed methyl ester (RME) blends. Initially, the performance of a solenoid-valve, common-rail injection system was be experimentally characterized, providing information about important parameters such as mass flow rate, momentum flux, injection velocity or spray cone angle for all fuels. After this, previously validated a theoretical spray model based on these parameters was used to predict internal spray structure, so that mixing characteristics can be compared for the three biodiesel blends. As far as air-fuel mixing indicators, characteristic mixing length and mixing time can be derived from the analyzed for the tested conditions.

The paper is structured in 6 sections. First, the experimental procedures and methodology are detailed. After this, the theoretical model used for the analysis of the mixing process development is described. Results of the characterization of the injection process are discussed in section 4. In the following section, a deep study of air-fuel mixing process is carried out. Finally, the most important conclusions of this work are established.

2. EXPERIMENTAL TOOLS

In the current paper the injection process will be characterized for different biodiesel blends using three parameters: mass flow rate, momentum flux and spray cone angle. The experimental set up used for this purpose will be described afterwards.

In these experiments, a standard common-rail injection system with a solenoid-valve injector was used. The nozzle has 8 conical orifices, with an outlet nominal diameter of 0.115 mm and k-factor of 1.5. The whole system is controlled by a Genotec impulse generator, simulating the function of the ECU (Electronic Control Unit).

The three fuels used for the study consist of two blends of standard diesel fuel and rapeseed methyl ester (RME) with a biodiesel mass percentage of 5 and 30%, as well as pure RME. The most significant diesel properties of these three fuels are detailed in Table 1. In the Table, the values of density, viscosity, surface tension and speed of sound are given for the fuels used. The distillation temperatures for 10%, 50% and 95% evaporated are also given. Surface tension and speed of sound for B30 were not determined.

2.1 Mass flow rate characterization

The injection rate measurements were carried out with a standard injection rate discharge curve indicator based in the Bosch method (anechoic tub), described in [14]. This device allows the measurement of the instantaneous mass flow rate given by the nozzle. In the current experiments, long injection pulses (2 ms) were used to characterize mass flow rate at stationary conditions (full needle lift). Although such an energizing time is not typical at all of normal driving conditions (not even for full load operation conditions), it makes possible the comparison of the injection process in controlled stationary conditions to be done.

In order to obtain a good estimation of the experimental errors, 25 repetitive measurements were carried out at the same test point (energizing time, rail pressure, and backpressure). Dispersion around 0.6% was obtained with proper calibration of the equipment.

2.2 Momentum flux measurement

The spray momentum is characterized by the measurement of the impingement strength of a spray on a surface. This strength is equivalent to the spray momentum flux, and can be determined with the use of the spray momentum test rig as presented in Payri *et al*. [15]. Sprays injected into a chamber can be pressurized with nitrogen up to 8 MPa in order to simulate pressure discharge conditions that are representative of real pressure conditions inside the engine combustion chamber during the injection process.

The measurement principle is shown in Figure 1. The impact strength is measured with a piezoelectric pressure sensor calibrated in order to measure strength and placed at 5 mm from the nozzle exit. The sensor frontal area and position are selected so that spray impingement area is much smaller than the area of the sensor. The pressure inside the chamber is constant and surrounds the entire spray, and fuel deflected is perpendicular to the direction of the axis. Under this assumption, and due to the conservation of momentum, the strength measured by the sensor is the same as the axial momentum flux at the hole outlet or at any other axial location.

2.3 Spray visualization test rig

For the macroscopic spray characterization, a specially constructed injection test rig is used. The test rig consists of a steel cube, including a chamber machined inside it. There are optical accesses in three of the cube faces, allowing different configurations for the flashes and cameras depending on the needs of the experiment. In Figure 2 a picture of the Nitrogen test rig is presented.

The test rig is designed to carry out experiments in non-reactive and non-evaporative conditions. For this, the test rig is filled with pressurized nitrogen, so that pressure inside the chamber can be fixed up to 6 MPa. Temperature can be controlled in a range between 15 and 50ºC, so evaporation is almost negligible during the experiments. Additionally, it is necessary to circulate the nitrogen through the rig in order to evacuate the fuel from the chamber, so that the quality of the images is maintained through the whole test.

2.4 Image acquisition and processing

Images are taken with a 12-bit CCD (*charge-coupled device*) camera (PixelFly by PCO). The spatial resolution for this camera is 1280x1024 pixels, with an exposure time of to 20 microseconds. A high power xenon flash is used for a proper illumination, with a flash duration of 8 microseconds. The camera is located on the opposite face of the injector and two flashes are used for lateral illumination, both facing each other providing a uniform illumination in the chamber.

Because of camera velocity limitations, each image corresponds to a different injection event. The injection and its synchronization with the camera and flash are managed by a specially constructed electronic system using the injector trigger signal as the reference to take the images. This system works at very low injection frequencies (0.25 Hz). The high time interval between injections is required for the N_2 flow to eliminate the fuel droplets from the previous injection and thus to keep good optical access for the spray.

A special software package is used for image processing. The segmentation algorithm is based on the log-likelihood ratio test (LRT). This method well suited indicated when boundary definition is difficult to do, as in the case of Diesel spray images. Moreover,

the method proved to be almost insensitive to intensity fluctuations between frames, providing better results than other algorithms. The influence of illumination quality was also evaluated in specific tests. The results demonstrated that this algorithm properly detects the estimated spray boundaries even in the case of comparatively poor illumination. Details of the image processing software are available in [16].

2.5 Test matrix

The aim of this paper is to evaluate the behavior of a standard injection system with different diesel-biodiesel blends. In order to make this comparison, mass flow rate and momentum flux measurements were performed for 5 different levels of injection pressure (30, 50, 80, 120 and 160 MPa) and 3 discharge pressures (2, 5 and 8 MPa), giving a total of 45 tests for each technique. The spray behavior was then characterized in terms of penetration and spray cone angle. Mass flow rate, momentum flux and visualization results are presented and discussed in section 4. The air-fuel mixing process was then evaluated using a theoretical model, which is described in section 3. This model uses as inputs the experimental data previously determined. The analysis of the air-fuel mixing process has been made for three different injection pressures, 50, 120 and 160 MPa and a backpressure of 2 MPa. The model results are discussed in section 5.

3. THEORETICAL APPROACH

Desantes *et al*. [17] proposed a theoretical model to calculate local spray characteristics based on the analogy between gas jets and diesel sprays. Momentum flux conservation was used to derive the following implicit equation to calculate velocity values in the spray axis U_{axis}:

$$\dot{M}_o = \frac{\pi}{2\alpha}\rho_a \tan^2\left(\frac{\theta_u}{2}\right) x^2 U_{axis}^2 \sum_{i=0}^{\infty} \frac{1}{\left(1+i\frac{Sc}{2}\right)}\left[\left(\frac{U_{axis}}{U_o}\right)\left(\frac{1+Sc}{2}\right)\left(\frac{\rho_f-\rho_a}{\rho_f}\right)\right]^i \quad (1)$$

where $\dot{M}_0$ and U_o are momentum flux and spray velocity at the nozzle outlet, ρ_a and ρ_f are the air and fuel densities, x is the axial coordinate, Sc is the *Schmidt* number (defined as the quotient between kinematic viscosity and mass diffusivity, $\left(Sc = \frac{\upsilon}{D}\right)$) and α is the shape factor for the Gaussian profiles used to described the local distribution of velocity and concentration inside the spray:

$$U(x,r) = U_{axis}(x)\exp\left(-\alpha\left(\frac{r}{R}\right)^2\right) \quad (2)$$

$$C(x,r) = C_{axis}(x)\exp\left(-\alpha Sc\left(\frac{r}{R}\right)^2\right) \quad (3)$$

with R being the spray radius defined by the spray cone angle θ_u, r the radial coordinate, and $C_{axis}(x)$ the mass concentration value at a determined axial position.

θ_u is the spray cone angle obtained from the velocity distribution profile. It is defined by the points placed in the periphery of the spray for which the local velocity has dropped to 1% of its value at the spray axis.

It can also be demonstrated that axial values of velocity and concentration can be related by the use of the *Schmidt* number:

$$C_{axis} = \left(\frac{1+Sc}{2}\right)\frac{U_{axis}}{U_o} \quad (4)$$

Thus, the previous equations can be used to determine the local distribution of velocity and mass concentration inside the spray at any position *(x, r)* if parameters such as

momentum flux, spray outlet velocity, spray cone angle or *Schmidt* number are previously characterized. It should be noted that the following conditions apply the equation (1):

- Cylindrical symmetry and Gaussian profiles are assumed for the microscopic spray characteristics.
- The environment is quiescent, and so no axis deflection exists.
- The air density in the injection chamber is constant during the whole injection process.
- The momentum flux, and thus, the injection velocity and the mass flow rate, are constant during the whole injection process.
- Slip between gas and liquid phases is negligible.

This theoretical model has been extensively validated both in the near-nozzle region, by means of x-ray mass distribution data [18] [19], and in the fully developed region, using velocity values obtained from PDPA (*Phase Doppler Particle Analyser*) measurements [20], showing in both cases a good agreement with experimental results.

4. RESULTS

4.1 Mass flow rate

As stated before, the mass flow rate through the nozzle exit was measured for three different fuels and several injection conditions. Long injection pulses were selected in order to assure that stationary conditions were reached. Figure 3 shows an example of the evolution of instantaneous mass flow rate for the three fuels at an injection pressure of 160 MPa and backpressure of 5 MPa.

As can be seen, despite there being a significant difference between the fuels in terms of density (see Table 1), the mass flow rate signals are very similar, with the mass flow

rate at stationary conditions slightly higher for the pure RME fuel (around 1.5%). The same conclusion can be established when analyzing the values of mass flow rate at full needle lift conditions for the rest of the experimental tests (depicted in Figure 4 with respect to the root of Δp, being Δp the difference between injection and discharge pressure). As can be seen, the stationary mass flow rate is slightly lower for the pure RME, which is the densest fuel, at low injection pressure conditions (30 and 50 MPa). When the injection pressure gets higher and the velocity increases, the mass flow obtained for all of the fuels becomes almost equal, with differences in the same range as the uncertainties involved in the experiment. Only at a very high injection pressure (160 MPa) does the pure RME show slightly higher mass flow values, although the differences are again almost negligible. Similar behavior of diesel and biodiesel fuels in terms of stationary mass flow rate has also been also seen in previous studies [21] [22].

In order to explain the slight differences observed for the three tested fuels in terms of mass flow rate at steady conditions, it is necessary to examine the equation which describes the behavior of this parameter in terms of pressure drop:

$$\dot{m}_f = C_d \rho_f A_o u_B \tag{5}$$

with $\dot{m}_f$ being the mass flow rate at stationary conditions, C_d the discharge coefficient, A_o the nozzle outlet section, and u_B the outlet velocity obtained using the *Bernoulli* equation:

$$u_B = \sqrt{\frac{2\Delta p}{\rho_f}} \tag{6}$$

Thus, mass flow rate at stationary conditions can be described using the following equation:

$$\dot{m}_f = C_d A_o \sqrt{2\Delta p \rho_f} \quad (7)$$

Taking into account equation (7), differences of around 2.8% would be expected in terms of mass flow rate due to the effect of the fuel density. Since the differences observed experimentally are considerably lower, as seen above, this behavior can only be explained by differences in the discharge coefficient.

In order to analyze this effect, the discharge coefficient was calculated using the experimental mass flow rate data as:

$$C_d = \frac{\dot{m}_f}{A_o \sqrt{2\Delta p \rho_f}} \quad (8)$$

Figure 5 represents the evolution of discharge coefficient for the three fuels and all the injection conditions in terms of Reynolds number, defined as:

$$Re = \frac{D_o u_{ef}}{\nu} \quad (9)$$

with D_o being the geometric outlet diameter, u_{ef} the effective outlet velocity obtained from momentum flux measurements, and ν the kinematic viscosity of the fuels.

As it can be seen, the discharge coefficient has an asymptotic evolution in terms of *Reynolds* number. This evolution has been described in previous studies in the literature [23]. As expected, the shape of this asymptotic curve depends only on the characteristics of the injection system, especially the nozzle geometry, so that the points corresponding to the different fuels collapse into a single curve.

Looking at Figure 5, it can be seen that when increasing the purity of the biodiesel (from B5 to B100), the Reynolds number obtained for the same tests conditions is

significantly reduced due to the influence of the fuel viscosity (see Table 1). As a consequence, the discharge coefficient gets significantly reduced as the percentage of RME increases in the fuel, especially at low injection pressures. This behavior of the discharge coefficient compensates for the expected evolution of mass flow rate if the effect of fuel density is exclusively considered, leading to similar values for the different fuels, as seen before.

The similar mass flow injected for the different fuel blends would lead to the conclusion that the torque obtained at rated power should be scaled in terms of the mass heating value. Other authors [7] have previously seen that the power differences between diesel fuel and RME are lower than it would be expected in terms of their mass heating values. In this sense, it is important to point out the following facts:

- Although the differences are small, the mass injected when using the pure biodiesel is higher, which partially compensates its lower heating capacity.

- Due to its higher viscosity, RME shows a slightly larger hydraulic delay. This implies that the actual start of injection occurs at a larger crank angle even though the injection is commanded at the same time, reducing the power obtained.

- Atomization and mixing processes, as well as the chemical kinetics, vary for the different fuels. This would lead to a different combustion process, which could have an impact on rated power conditions. Further analysis would need to be done in this sense.

4.2 Momentum flux and effective velocity

The momentum flux was characterized for the same conditions as the mass flow rate. The stationary values of momentum flux with respect to the difference between injection and discharge pressure are plotted in Figure 6. Similar to the result for mass flow rate, values given by the nozzle for the three fuels are strongly similar.

The momentum flux can be defined as the product of the mass flow rate and the outlet velocity. Thus, the effective outlet velocity at stationary conditions can be calculated as the quotient of these two quantities. This result is shown in Figure 7. Since small differences were seen in the mass flow rate and the momentum flux behavior, the velocity values obtained are also quite similar for the tested fuels.

4.3 Spray visualization

Figure 8 shows the appearance of the injected sprays for B5 and B100 fuels at an injection pressure of 50 MPa and a chamber pressure of 2 MPa. The sprays presented for the two fuels were obtained at the same time after the start of injection. A preliminary evaluation of this image would lead to the conclusion that the biodiesel fuel shows slightly narrower and longer sprays than the diesel-RME blend. Nevertheless, in order to quantify these features the image processing technique described in section 2.4 was used. Figure 9 shows the spray penetration and spray angle values obtained using this methodology for the case of 50 MPa of injection pressure and 2 MPa of backpressure. Paying attention to the penetration curve, it can be seen that the B5 and B30 fuels show very similar values, while the penetration of B100 is significantly higher. An opposite behavior is detected for the spray cone angle, where the lowest values are reached for the B100 fuel. This is expected since penetration and cone angle are coupled by the following expression in the far field region:

$$S = K\dot{M}_o^{1/4}\rho_a^{-1/4}t^{1/2}\tan^{-1/2}\left(\frac{\theta_u}{2}\right) \quad (10)$$

where *K* is an universal constant with a value of 1.26 [24]. Thus, as the momentum flux is similar for the three fuels, a narrower spray cone angle implies a higher tip penetration.

The same behavior is observed when increasing injection pressure (Figure 10), and it has been observed also by other authors previously [25-27]. A possible explanation of this phenomenon could be related to the atomization efficiency. Lee *et al*. [28] and Kamrak*et al*. [29] have observed that the Sauter Mean Diameter (SMD) of droplets is significantly higher for biodiesel fuels, probably due to their higher surface tension. Higher droplet diameters can lead to higher inertial effects, which would imply higher penetrations, and poorer air entrainment, which affects mixing efficiency and spray cone angle.

5. ANALYSIS OF AIR-FUEL MIXING PROCESS

5.1 Characteristic mixing length and time

In a previous study [30], the authors developed a theoretical analysis to describe the characteristic mixing length and time based on the movement of a fuel parcel inside a quasi-steady turbulent spray. The following expressions were found:

$$x_m = \frac{kC_a^{1/2}D_o\rho_f^{1/2}}{C_m\rho_a^{1/2}\tan\left(\frac{\theta_u}{2}\right)} \quad (11)$$

$$t_m = \frac{kC_a^{1/2}D_o\rho_f^{1/2}}{C_m^2u_{ef}\rho_a^{1/2}\tan\left(\frac{\theta_u}{2}\right)} \quad (12)$$

where k is a constant term, x_m and tm are the characteristic mixing length and time respectively, C_m is the characteristic mixing concentration achieved in the spray axis at the axial position x_m and C_a is the area coefficient, defined as:

$$C_a = \frac{A_{ef}}{A_o} \tag{13}$$

with A_{ef} being the effective outlet section of the nozzle, obtained from momentum flux measurements.

In order to compare these parameters between the different fuels, the mixing length and time can be compared for a generic mixing concentration C_m, that will be considered as equal for all the fuels.

This information can be seen in Figures 11 and 12. In order to see more directly the differences between the fuels, the values of x_m and t_m are presented divided by the B5 values, which is used as the reference fuel. In terms of mixing length, it can be seen that in general terms B5 and B30 show similar behavior, except in the case of the 120 MPa injection pressure, due to its lower spray angle value. Nevertheless, greater differences are found for the pure biodiesel fuel, with the pure biodiesel showing a loss in efficiency in terms of air-fuel mixing. Similar conclusions were found in terms of mixing time.

5.2 Local velocity and concentration contours

The theoretical model described in section 3 can be used to calculate local velocity and concentration inside the spray as a means to explore the air-fuel mixing process. For this purpose, data from the previous experimental results were used (momentum flux, effective outlet velocity, and spray con angle). Nevertheless, regarding equation (1), there is still an important parameter which remains unknown: the Schmidt number.

Recently, Salvador et al. [19] have used X-ray mass distribution measurements and the theoretical model described previously to estimate a range between 0.5 and 0.6 for the Schmidt number in Diesel sprays. Thus, for the present study, a value of 0.55 was chosen.

The information obtained by the model is shown in contour plots for two different injection conditions: injection pressures of 50 and 160 MPa and a backpressure of 2 MPa (Figures 13 and 14, respectively). As far as the velocity contours are concerned, it can be seen that pure biodiesel fuel shows narrower and longer regions for the same local velocity values than the diesel-biodiesel blends (B5 and B30). This behavior can be explained in terms of the lower spray angle values observed for the B100 fuel, which indicates that air entrainment is considerably lower with respect to the other fuels. Since momentum flux is conservative and very similar between the different fuels, higher local velocities are expected.

Related to the concentration contours, slight differences are noticeable between the two diesel-biodiesel blends (B5 and B30) in terms of mixing efficiency. Contrarily, the pure biodiesel fuel shows narrower and longer regions for the same concentration values, which indicates that the air-fuel mixing is less efficient. Thus, the spray combustion would take place at larger positions, near the combustion chamber walls, and so, with a significant influence on pollutant formation.

It is important to consider that, besides spray formation, fuel composition affects also the stoichiometric air-fuel ratio. This parameter varies from $\frac{1}{14.5}$ for a standard diesel fuel to $\frac{1}{12.5}$ for pure RME. Figures 15 and 16 represent the iso-concentration lines for the three fuels tested and two different concentration values: 0.01 (the concentration which defines spray cone angle) and the stoichiometric concentration, which marks the region

at which combustion would start. As can be seen, due to the chemical characteristics of the fuels, the differences in terms of stoichiometric conditions for a given location are reduced with respect to the behavior observed previously. Anyway, it can also be seen that the stoichiometric region is narrower for the pure biodiesel, although the difference is small.

6. CONCLUSIONS

In this paper, a complete analysis of the injection system behavior and the air-fuel mixing process when using different diesel-RME blends (biodiesel percentage of 5, 30 and 100%) was carried out. For this purpose, the mass flow rate and the momentum flux have been measured to characterize the hydraulic behavior of a standard common-rail injection system with the three different fuels. The tests have been developed with long injection pulses, in order to achieve quasi-steady conditions. From this analysis, the following conclusions can be drawn:

- Despite biodiesel is fuel higher density, the mass flow rate measurements obtained are strongly similar, and only slight differences are found for the pure rapeseed methyl ester fuel.
- As seen before in the literature, the discharge coefficient has an asymptotic behavior with respect to Reynolds number, increasing as Re gets higher. Due to their higher viscosity, blends with a higher percentage of biodiesel show lower values of Reynolds number for the same pressure conditions, so that discharge coefficient is significantly lower, especially at low injection pressures. The effect of the discharge coefficient compensates for the effect of density, leading to similar stationary mass flow rates, as stated before.

- The measured momentum fluxes are similar for the three fuels, as it was seen with the mass flow rates. As a consequence, similar outlet effective velocities were also found.

Together with the hydraulic characterization, spray visualization tests were developed for several conditions. It can be immediately seen that blends with low percentage of RME behave similarly, while pure biodiesel shows significantly higher spray penetration and lower spray angle. This is an indicator of a less efficient air-fuel mixing process, probably due to a poorer atomization of the fuel, as introduced in previous studies. Furthermore, turbulent spray theory was used to estimate characteristic mixing lengths and times for the tested conditions. Higher values of these parameters are obtained for the RME fuel, while B5 and B30 behave similar.

Finally, in order to further analyze mixing process, a theoretical spray model has been used. This model allows obtaining the distribution of mass concentration and velocity in the spray. Paying attention to these distributions, it can be seen that the biodiesel shows higher fuel concentrations and higher local velocities with respect to the blends in the same spray positions. Again, this fact is a consequence of a poorer mixing process.

Nevertheless, when looking for the contours which define the stoichiometric air-fuel ratio for the three fuels, they are placed very close to each other, which would mean that the differences found in terms of air-fuel mixing process are compensated by the differences in the fuel composition.

ACKNOWLEDGMENTS

This work was partly sponsored by *"Vicerrectorado de Investigación, desarrollo e Innovación"* of the "*Universitat Politècnica de Valencia*" in the frame of the Project "*Estudio del flujo en toberas de inyección diesel mediante técnicas LES*

(LESFLOWGRID)", *Reference Nº 2837* and by *"Ministerio de Ciencia e Innovación"* in the frame of the Project *"Estudio teórico-experimental sobre la influencia del tipo de combustible en los procesos de atomización y evaporación del chorro Diesel (PROFUEL"), Reference TRA2011-26293*. This support is gratefully acknowledged by the authors.

REFERENCES

[1] Altin R, Cetinkaya S, Yucescu HS. The potential of using vegetable oil fuels as fuel for diesel engines. Energy Conversion and Management 2001; 42 (5): 529-538.

[2] Rakopoulos CD, Antonopoulos KA, Rakopoulos DC, Hountales DT, Giakoninis EG. Comparative performance and emissions study of a direct injection Diesel engine using blends of Diesel fuel with vegetable oils or bio-diesels of various origins. Energy Conversion and Management 2006; 47 (18-19): 3272-3287.

[3] Agarwal AK. Biofuels (alcohols and biodiesel) applications as fuels for internal combustion engines. Progress in Energy and Combustion Science 2007; 33(3): 233-271.

[4] Basha SA, Gopal KR, Jebaraj S. A review on biodiesel production, combustion, emissions and performance. Renewable & Sustainable Energy Reviews 2009; 13(6-7): 1628-1634.

[5] Luján JM, Bermúdez V, Tormos B, Pla B. Comparative analysis of a DI diesel engine fuelled with biodiesel blends during the European MVEG-A cycle: Performance and emissions (II). Biomass Bioenerg 2009; 33 (6-7): 948-956.

[6] Golovitchev VI, Yang J. Construction of combustion models for rapeseed methyl ester bio-diesel fuel for internal combustion engine applications. Biotechnology Advances 2009; 27: 641-655.

[7] Lapuerta M, Armas O, Rodríguez-Fernández J. Effect of biodiesel fuels on diesel engine emissions. Progress in Energy and Combustion Science 2008; 34 (2): 198-223.

[8] Badock C, Wirth R, Tropea C. The influence of hydro-grinding on cavitation inside a Diesel injection nozzle and primary break-up under unsteady conditions. Proc. ILASS-Europe 99; Toulouse, July 1999.

[9] Ning W, Reitz R, Diwakar R, Lipper A. A numerical investigation of nozzle geometry and injection conditions effects on diesel fuel injector flow physics. SAE Paper 2008; 2008-01-0936.

[10] Payri F, Bermúdez V, Payri R, Salvador FJ. The influence of cavitation on the internal flow and the spray characteristics in diesel injection nozzles. Fuel 2004; 83: 419-431.

[11] Jung K, Khil T, Yoon Y. Effects of orifice internal flow on breakup characteristics of like-doublet injectors. Journal of Propulsion and Power 2006; 22 (3): 1329-1339.

[12] Naber JD, Siebers DL. Effects of gas density and vaporization and penetration and dispersion of diesel sprays. SAE Paper 1996; 960034.

[13] Park S, Suh H, Lee C. Effect of cavitating flow on the flow and fuel atomization characteristics of biodiesel and diesel fuels. Energy & Fuels 2008; 22: 605-613.

[14] Bosch W. The fuel rate indicator: a new measuring instrument for display of the characteristics of individual injection. SAE Paper 1966; 660749.

[15] Payri R, Garcia JM, Salvador FJ, Gimeno J. Using spray momentum flux measurements to understand the influence of diesel nozzle geometry on spray characteristics. Fuel 2005; 84: 551-561.

[16] Pastor JV, Arrègle J, García JM, Zapata LD. Segmentation of diesel spray images with log-likelihood radio test algorithm for non-gaussian distributions. Applied Optics 2006; 46 (6): 888-899.

[17] Desantes JM, Payri R, García JM y Salvador FJ. A contribution to the understanding of isothermal diesel sprays. Fuel 2007; 86 (7-8): 1093-1101.

[18] Desantes JM, Salvador FJ, López JJ, De la Morena J. Study of mass and momentum transfer in diesel sprays based on X-ray mass distribution measurements and on a theoretical derivation. Exp Fluids 2011; 50:233–246

[19] Salvador FJ, Ruiz S, Gimeno J, De la Morena J. Estimation of a suitable Schmidt number range in diesel sprays at high injection pressure. International Journal of Thermal Sciences 2011; 50: 1790-1798.

[20] Payri R, Tormos B, Salvador FJ, Araneo L. Spray droplet velocity characterization for convergent nozzles with three different diameters. Fuel 2008; 87: 3176-3182.

[21] Luján JM, Tormos B, Salvador FJ, Gargar K. Comparative analysis of a DI diesel engine fuelled with biodiesel blends during the European MVEG-A cycle: Preliminary study (I). Biomass Bioenerg 2009; 33 (6-7): 941-947.

[22] Salvador FJ, Martínez-López J, Romero JV Roselló MD. Influence of biofuels on the internal flow in diesel injector nozzles. Mathematical and Computer Modelling 2011; 54: 1699–1705.

[23] Lichtarowicz A, Duggins RK, Markland E. Discharge coefficients for incompressible non-cavitating flow through long orifices. Journal of Mechanical Engineering Science 1965; 7 (2): 210-219.

[24] Desantes JM, Payri R, Salvador FJ, Gil A. Development and validation of a theoretical model for diesel spray penetration. Fuel 2006; 85: 910-917.

[25] Wang XG, Huang ZH, Kuti OA, Zhang W, Nishida K. Experimental and analytical study on biodiesel and diesel spray characteristics under ultra-high injection pressure. Int J Heat Fluid Flow 2010; 31: 659-666.

[26] Podorevc P, Kegl B, Skerget, L. Diesel and biodiesel fuel spray simulations. Energy Fuels 2008; 22 (2): 1266-1274.

[27] Gao Y, Deng J, Li C, Dang F, Liao Z, Wu Z, Li L. Experimental study of the spray characteristics of biodiesel based on inedible oil. Biotechnology Advances 2009; 27: 616-624.

[28] Lee CS, Park SW, Kwon SI. An Experimental Study on the Atomization and Combustion Characteristics of Biodiesel-Blended Fuels. Energy Fuels 2005; 19: 2201-2208.

[29] Kamrak J, Kongsombut B, Grehan G, Saengkaew S, Kim K-S, Charinpanitkul T. Mechanistic study on spraying of blended biodiesel using phase Doppler anemometry. Biomass Bioenerg 2009; 33 (10): 1452-1457.

[30] Payri R, Salvador FJ, Gimeno J, Zapata LD. Diesel nozzle geometry influence on spray liquid-phase fuel penetration in evaporative conditions. Fuel 2008; 87: 1165-1176.

LIST OF TABLE AND FIGURE CAPTIONS

Figure 15: Contours for stoichiometric conditions. P_{inj}: 50 MPa

Figure 16: Contours for stoichiometric conditions. P_{inj}: 120 MPa

Fuel	*% RME* (in mass)	*Density* $[kg/m^3]$ (at 15ºC)	*Viscosity* $[mm^2/s]$ (at 40ºC)	$T_{10\%}[ºC]$	$T_{50\%}[ºC]$	$T_{95\%}[ºC]$	*Surface Tension [N/m]*	*Speed of sound [m/s] (at 25ºC)*
B5	5%	831±0.2	2.38 ±0.42	195 ±3.9	272 ±3.9	348 ±3.9	0.0205	1338.7
B30	30%	851±0.2	3.12 ±0.42	214 ±3.9	307 ±3.9	345 ±3.9	ND	ND
B100	100%	879±0.2	4.47 ±0.42	336 ±3.9	340 ±3.9	355 ±3.9	0.028	1377.6

Table 1: properties of the fuels at atmospheric pressure

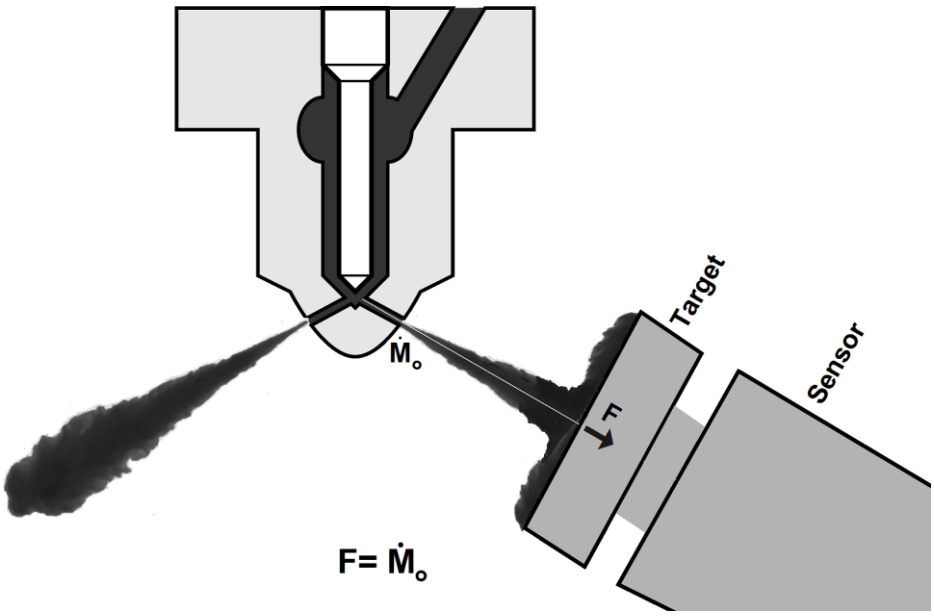

Figure 1: Momentum flux measuring principle

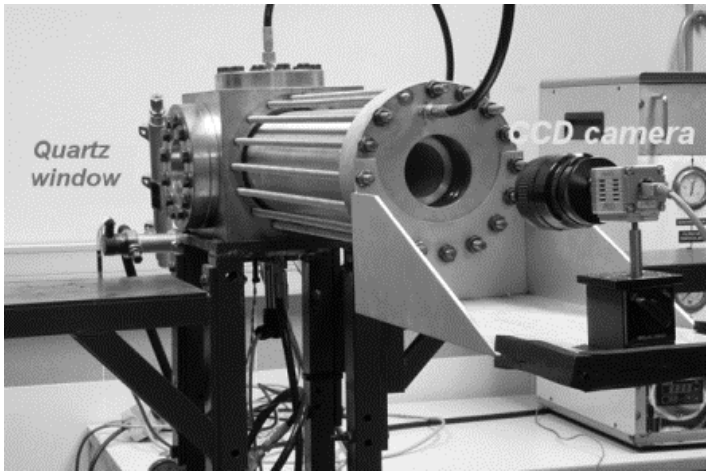

Figure 2: Visualization test rig

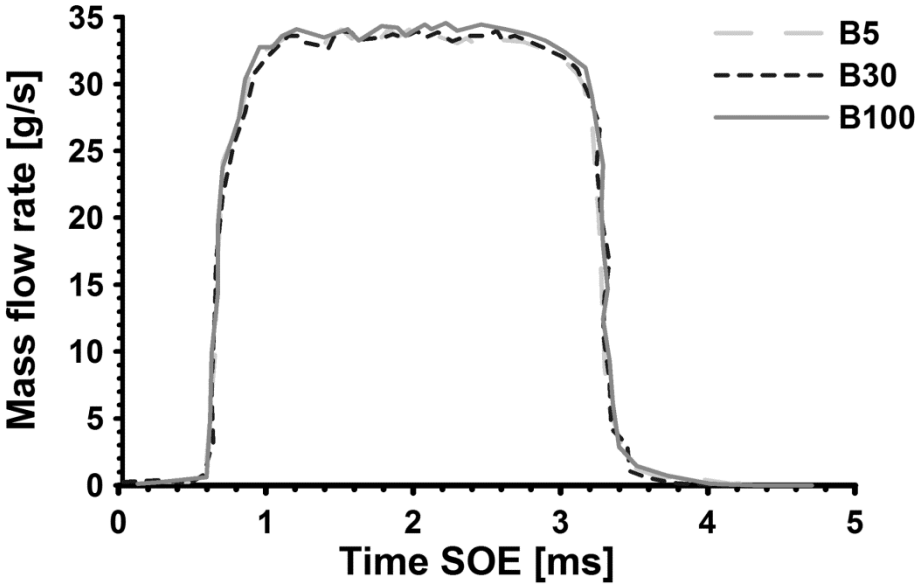

Figure 3: Mass flow rate signal. P_{inj}: 160 MPa, P_b: 5 MPa

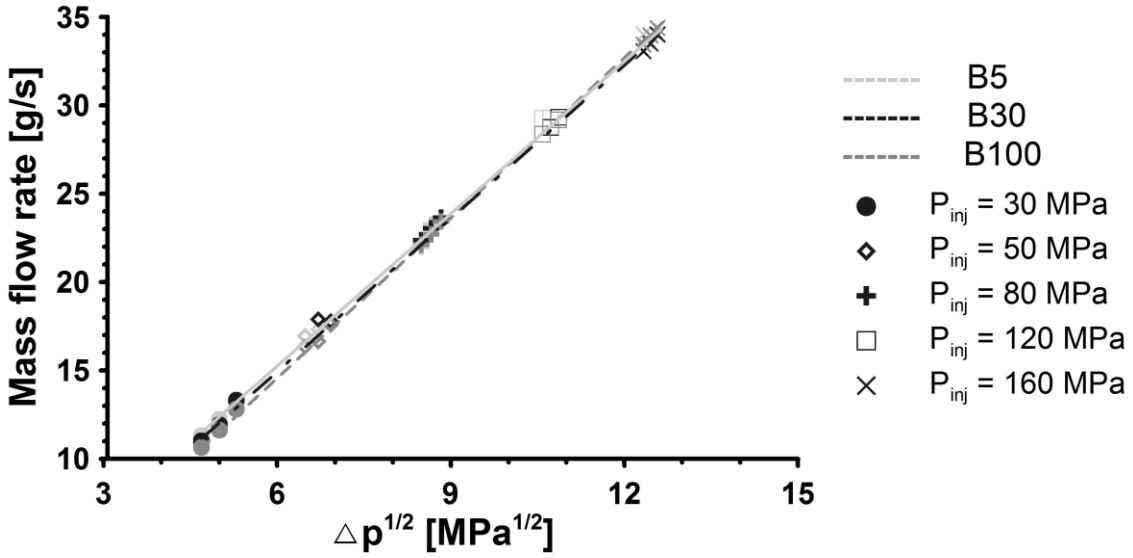

Figure 4: Stationary mass flow rate vs. the root of Δp

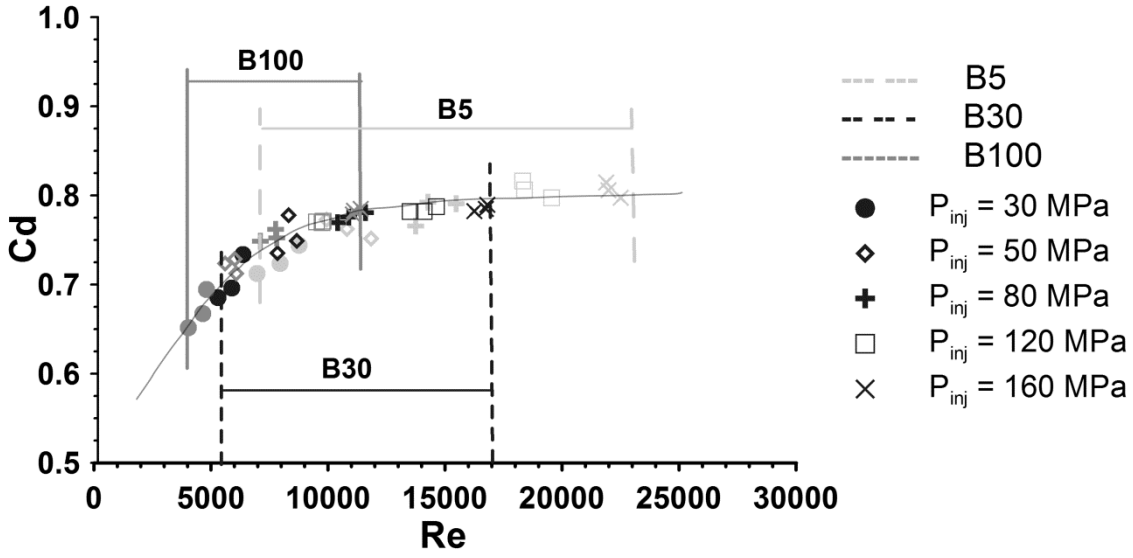

Figure 5: Evolution of the discharge coefficient with respect to the *Reynolds* number

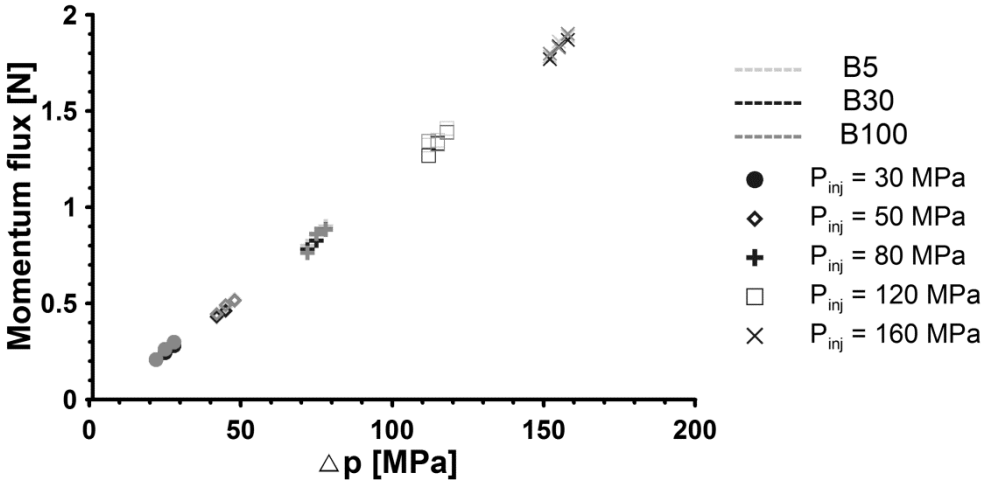

Figure 6: Stationary momentum flux vs. Δp

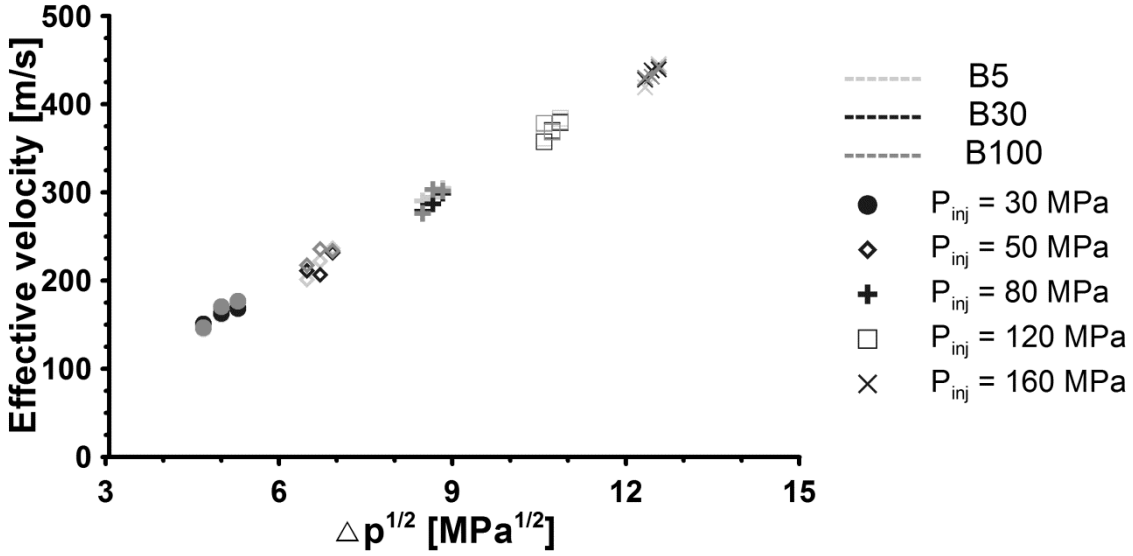

Figure 7: Outlet effective velocity vs. the root of Δp

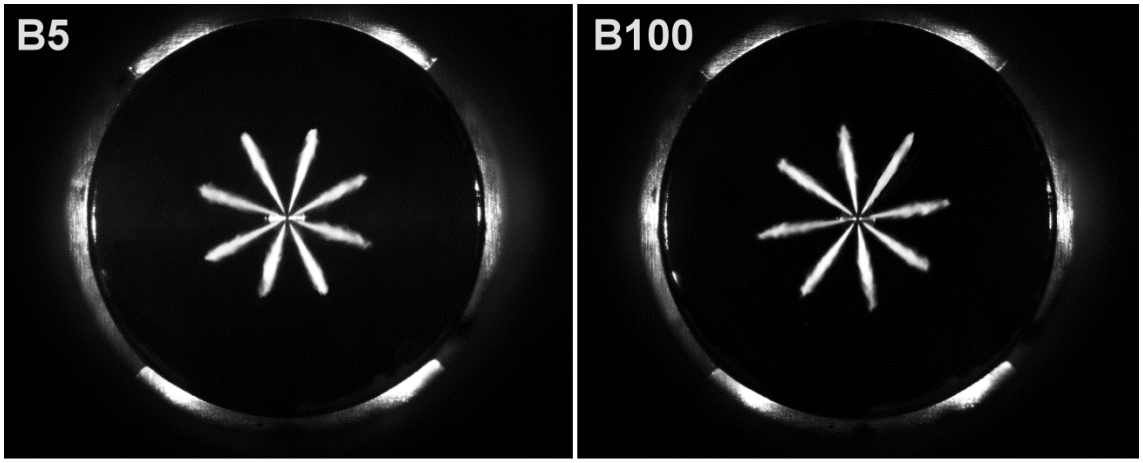

Figure 8: Spray image for B5 (left) and B100 (right). P_{inj}: 50 MPa, P_b: 2.1 MPa

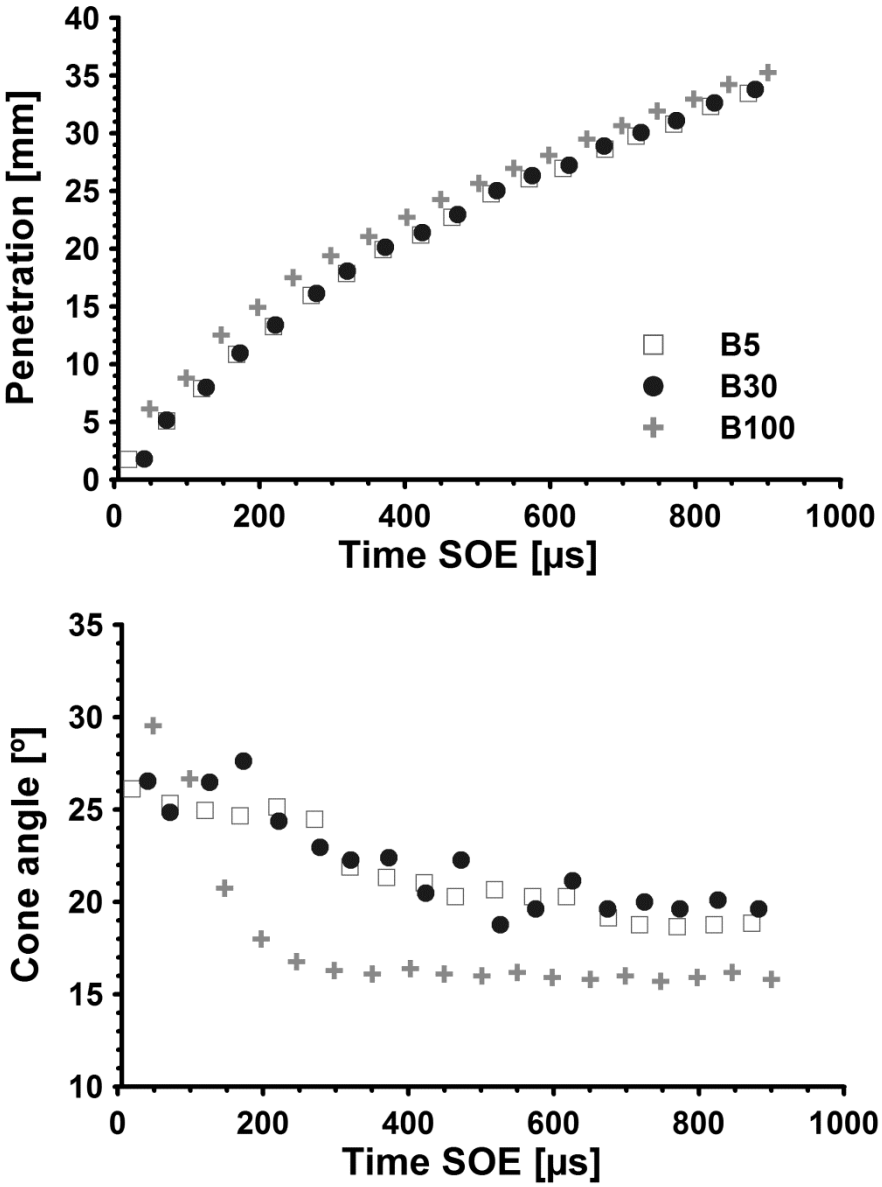

Figure 9: Visualization results for P_{inj}: 50 MPa and P_b: 2 MPa

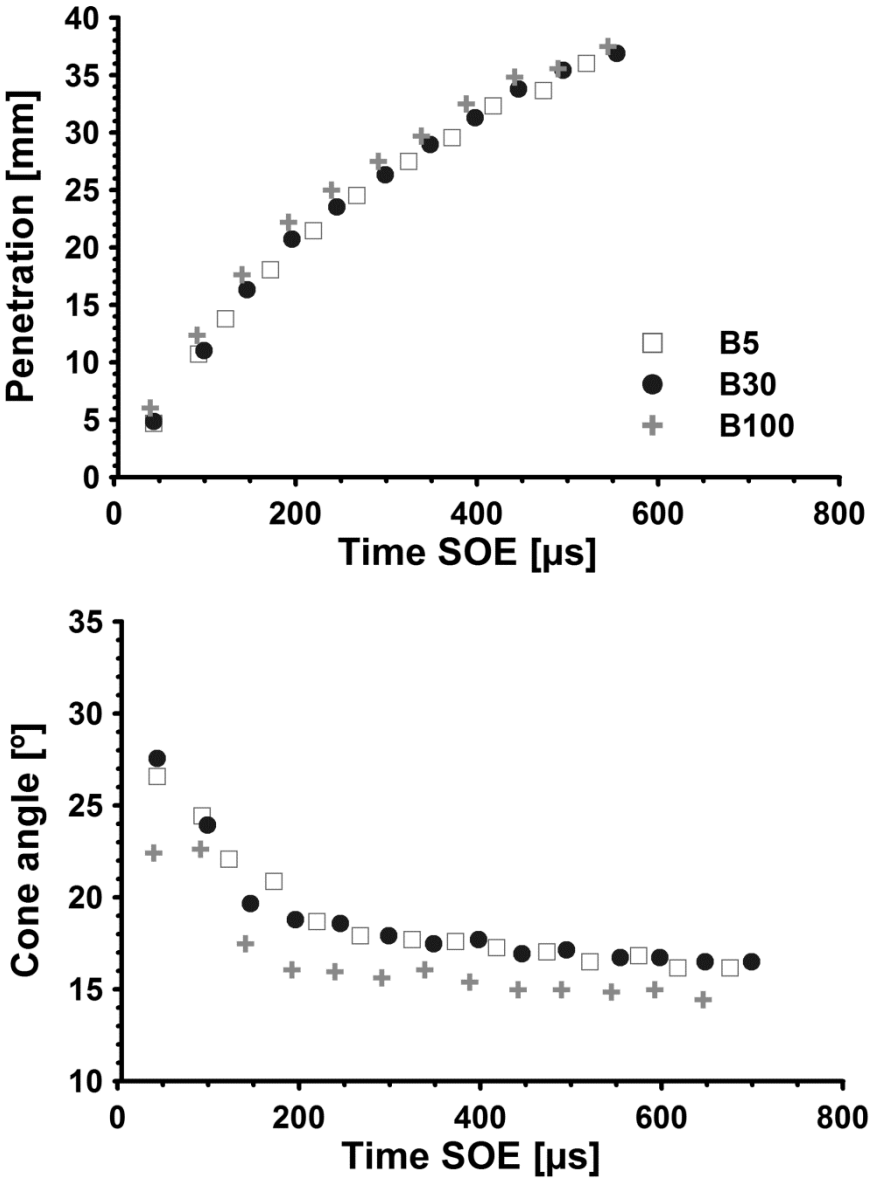

Figure 10: Visualization results for P_{inj}: 160 MPa and P_b: 2 MPa

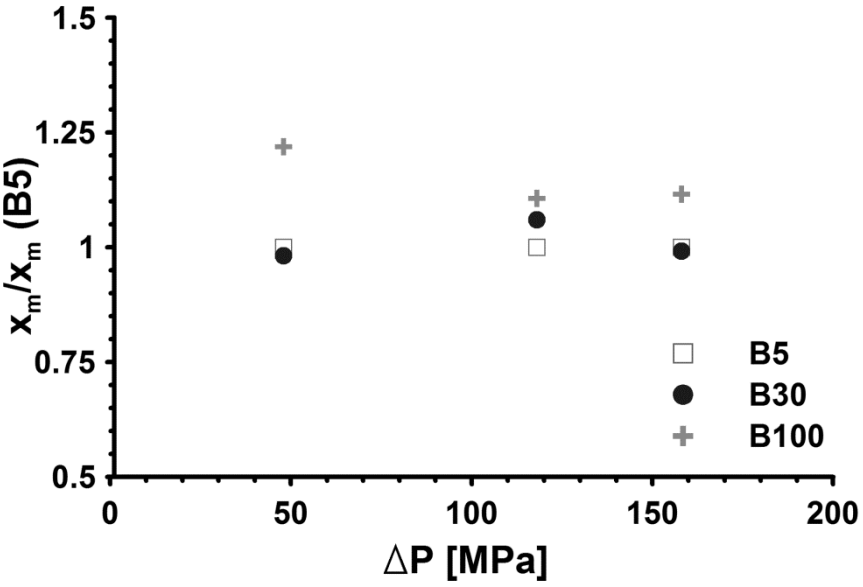

Figure 11: Modified characteristic mixing length adimensionalized by B5 values

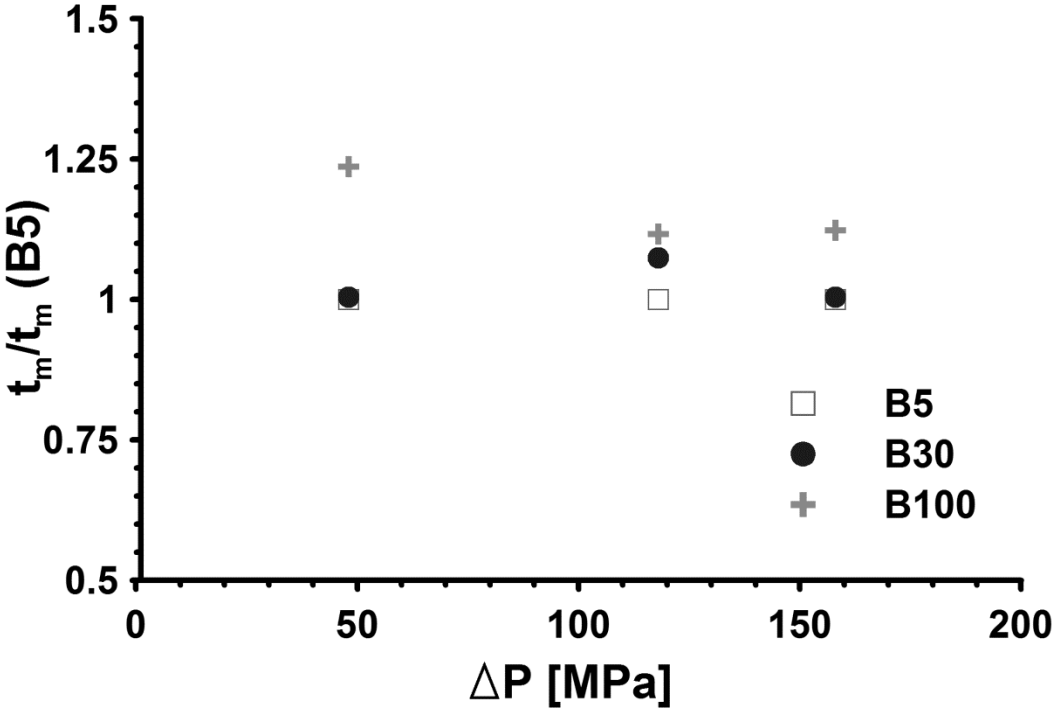

Figure 12: Modified characteristic mixing time adimensionalized by B5 values

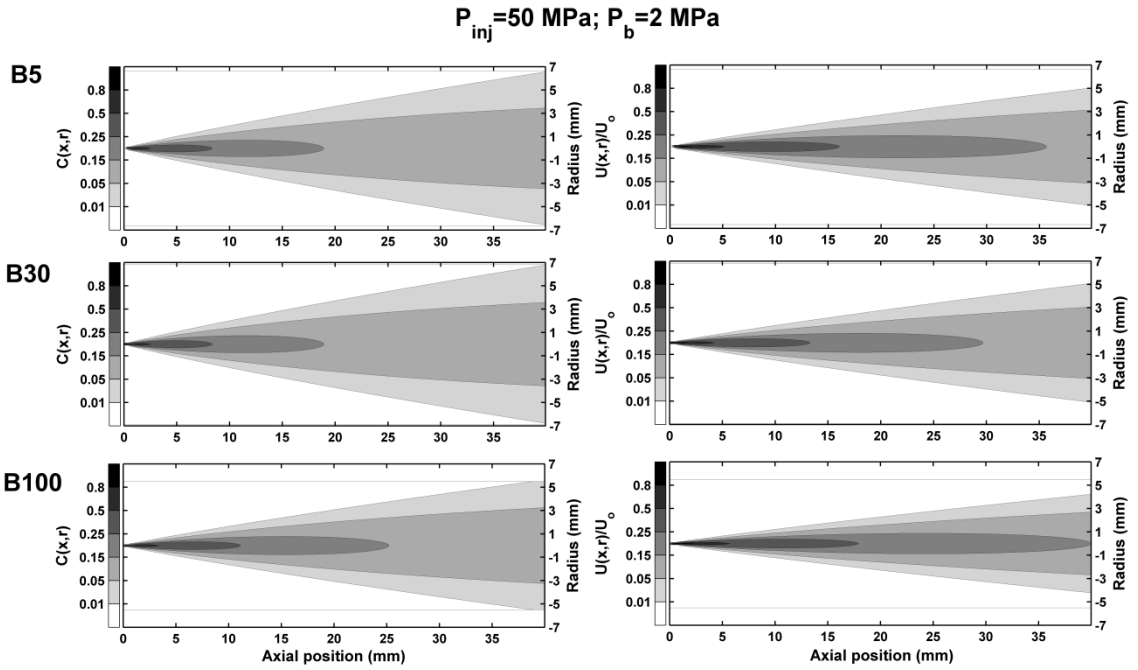

Figure 13: Local velocity and concentration contours obtained from the theoretical model. P_{inj}: 50 MPa

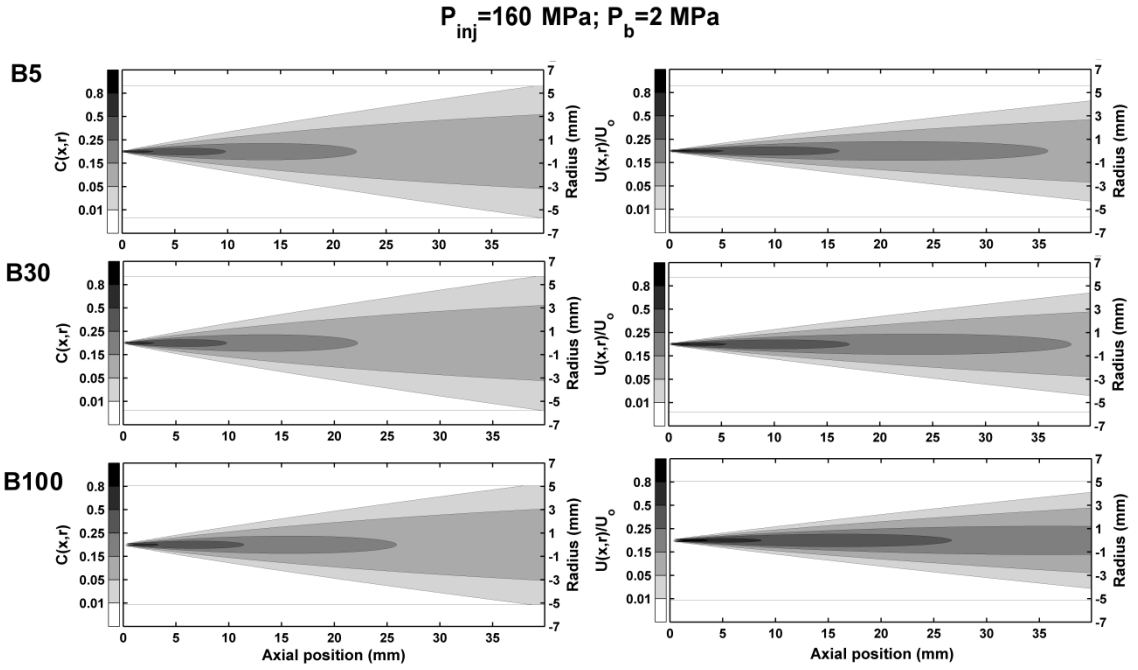

Figure 14: Local velocity and concentration contours obtained from the theoretical model. P_{inj}: 160 MPa

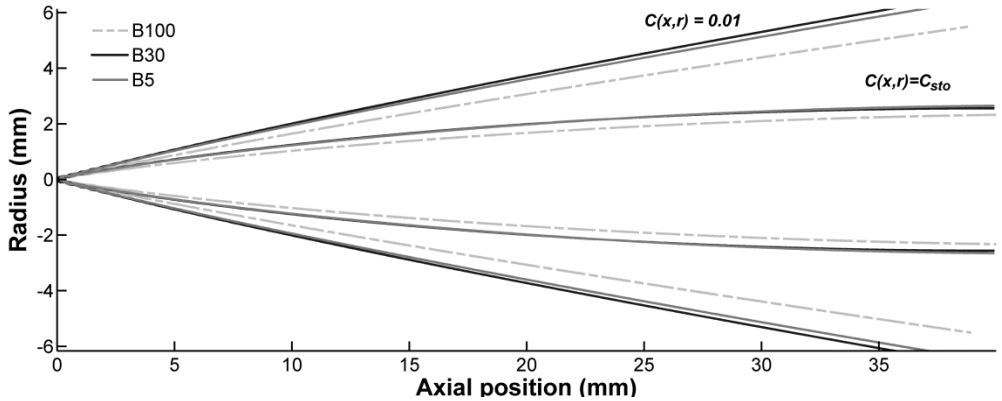

Figure 15: Contours for stoichiometric conditions. P_{inj}: 50 MPa

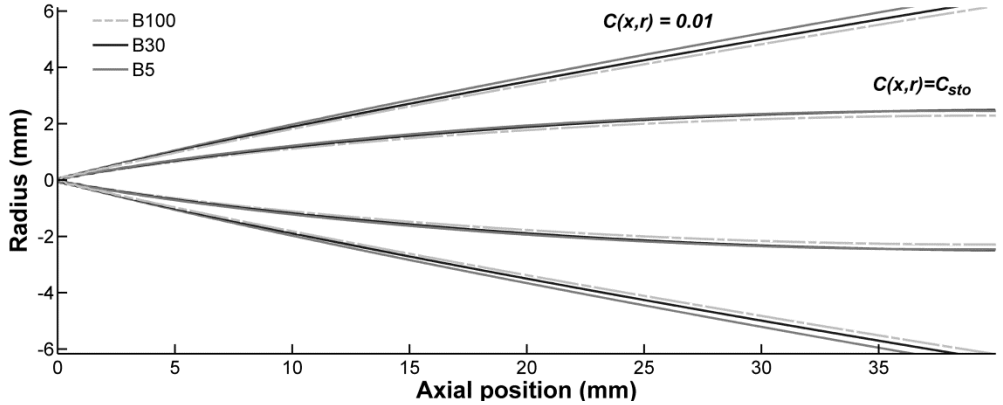

Figure 16: Contours for stoichiometric conditions. P_{inj}: 120 MPa

NOTATION

A_0: *Geometric outlet area*

A_{ef}: *Effective outlet area*

C(x,r): *Spray local concentration at x axial position and r radial position*

$C_{axis}(x)$: *Spray mass concentration in the spray axis at axial position x*

C_a: *Area coefficient*

C_d: *Discharge coefficient*

C_m: *Characteristic mixing spray concentration*

D: *Mass diffusivity*

D_i: *Geometric nozzle inlet diameter*

D_o: *Geometric nozzle outlet diameter*

f: *Generic radial function for spray velocity distribution*

i: *Counter in the Taylor series*

K: *Constant term for the spray penetration correlation*

k: *Constant term for the characteristic mixing length and time equations*

k-factor: *Nozzle conicity, defined as* $k - factor = \frac{D_i - D_o}{10}$

$\dot{m}_f$: *Mass flow*

$\dot{M}_0$: *Momentum flux at the nozzle exit*

P_{inj}: *Injection pressure*

P_b: *Discharge pressure*

r: *Radial position in the spray*

R: *Spray radius at a given axial position x*

Re: *Reynolds number*

S: *Spray penetration*

Sc: *Schmidt number*

t: *Time elapsed from start of injection*

t_m*:* *Characteristic mixing time*

U(x,r): *Spray local velocity at x axial position and r radial position*

$U_{axis}(x)$*:* *Spray velocity in the spray axis at axial position x*

U_0*:* *Spray velocity at the nozzle outlet*

u_B*:* *Theoretical outlet velocity given by Bernoulli equation*

u_{ef}*:* *Effective outlet velocity*

x: *Axial position in the spray*

x_m*:* *Characteristic mixing length*

Greek symbols

α: *Coefficient of the Gaussian radial profile for the axial velocity*

ΔP: *Pressure drop,* $\Delta P = P_{inj} - P_b$

θ_u*:* *Spray velocity angle*

ρ_a*:* *Air density*

ρ_f*:* *Fuel density*

υ: *Kinematic viscosity*